Available online at www.sciencedirect.com
ScienceDirect
Surface Science 601 (2007) 1008–1018
SURFACE SCIENCE
www.elsevier.com/locate/susc

Metal organic chemical vapor deposition of ultrathin ZrO_2 films on Si(1 0 0) and Si(1 1 1) studied by electron spectroscopy

P.G. Karlsson [a], J.H. Richter [a], J. Blomquist [b], P. Uvdal [b], T.M. Grehk [c], A. Sandell [a,*]

[a] *Department of Physics, Uppsala University, Box 530, SE-75121 Uppsala, Sweden*
[b] *Chemical Physics, Lund University, Box 118, SE-22100 Lund, Sweden*
[c] *Materials Science, Högskolan Dalarna, SE-781 88 Borlänge, Sweden*

Received 22 September 2006; accepted for publication 22 November 2006
Available online 11 December 2006

Abstract

The growth of ultrathin ZrO_2 films on Si(1 0 0)-(2 × 1) and Si(1 1 1)-(7 × 7) has been studied with core level photoelectron spectroscopy and X-ray absorption spectroscopy. The films were deposited sequentially by chemical vapor deposition in ultra-high vacuum using zirconium tetra-*tert*-butoxide as precursor. Deposition of a > 50 Å thick film leads in both cases to tetragonal ZrO_2 (*t*-ZrO_2), whereas significant differences are found for thinner films. On Si(1 1 1)-(7 × 7) the local structure of *t*-ZrO_2 is not observed until a film thickness of 51 Å is reached. On Si(1 0 0)-(2 × 1) the local geometric structure of *t*-ZrO_2 is formed already at a film thickness of 11 Å. The higher tendency for the formation of *t*-ZrO_2 on Si(1 0 0) is discussed in terms of Zr–O valence electron matching to the number of dangling bonds per surface Si atom. The Zr–O hybridization within the ZrO_2 unit depends furthermore on the chemical composition of the surrounding. The precursor *t*-butoxy ligands undergo efficient C–O scission on Si(1 0 0), leaving carbonaceous fragments embedded in the interfacial layer. In contrast, after small deposits on Si(1 1 1) stable *t*-butoxy groups are found. These are consumed upon further deposition. Stable methyl and, possibly, also hydroxyl groups are found on both surfaces within a wide film thickness range.

Keywords: High dielectrics; Zirconium dioxide; Silicon; Chemical vapor deposition; Semiconductor–insulator interfaces; Synchrotron radiation photoelectron spectroscopy; X-ray absorption spectroscopy

1. Introduction

High dielectric constant metal oxides have attracted considerable attention lately as potential replacements to SiO_2 as gate material in metal-oxide semiconductors field effect transistors (MOSFETs) [1]. A replacement is needed since the limit for the miniaturization of silicon based MOSFET devices is rapidly approaching. When the gate insulating film of these devices is thinner than 5 nm quantum mechanical tunneling currents across the film becomes significant. One way to achieve additional scaling is to replace SiO_2 with a material with a higher dielectric constant. A high-dielectric constant gate material can be physically thicker, reducing leakage currents while maintaining the electrical properties. ZrO_2 has emerged as a possible replacement to SiO_2 as gate material. ZrO_2 has a dielectric constant of about 20, which is five times that of SiO_2. It has been demonstrated that MOS devices fabricated using ZrO_2 as dielectric have most promising electrical characteristics [2,3].

The metal-organic chemical vapor deposition (MOCVD) technique is well adapted to realize films that meet the criteria for a functioning device. MOCVD growth allows for atomic layer control of the film thickness along with other appealing properties, such as uniform thickness of large areas, stoichiometric control and excellent conformal step coverage of non-planar devices [4,5]. A proper choice of precursor furthermore allows for film growth at low temperatures with a satisfactory deposition rate, making the method economically viable.

* Corresponding author. Tel.: +46 18 471 35 48; fax: +46 18 471 35 24.
E-mail address: anders.sandell@fysik.uu.se (A. Sandell).

0039-6028/$ - see front matter © 2006 Elsevier B.V. All rights reserved.
doi:10.1016/j.susc.2006.11.038

CVD of ZrO_2 has been performed using several different precursors [6–10]. Among metal-organic precursors, zirconium tetra-*tert*-butoxide [$Zr(OC(CH_3)_3)_4$, (ZTB)] appears particularly attractive. It has a high vapor pressure and decomposes to form ZrO_2 without an additional oxidant at substrate temperatures as low as 300 °C [10]. Previous studies of ZTB-mediated CVD of ZrO_2 on the Si(1 0 0) surface have addressed important issues on the interface and electric properties, thermal stability, growth mechanism and band alignment [11–20]. Film growths using ZTB as single source precursor and ZTB with the addition of O_2 have been explored.

Most valuable information on the formation of thin metal oxide films by way of MOCVD can be obtained by studies under ultra-high vacuum (UHV) conditions using surface science methodology [21–23]. Photoelectron spectroscopy (PES) and X-ray absorption spectroscopy (XAS) are tools extremely well suited for studies of film growth and interface formation as they provide information on the chemical composition, chemical state of specific elements as well as a map of the frontier electronic levels. Thus a detailed picture of the evolution of the electronic and geometric properties of the metal oxide film and the metal oxide–substrate interface can be obtained by monitoring changes in the electronic core and valence spectra for films of increasing thickness.

Recently, we presented a study of ZTB-mediated growth of ZrO_2 on Si(1 0 0) that reported on film thickness dependent variations in the band alignment based on PES and XAS results [24]. In the present paper, we continue the work on ZrO_2 UHV-MOCVD growth on silicon surfaces. The emphasis is now placed on precursor fragmentation and the electronic and geometric properties of the first few oxide layers. The discussion is mainly centered on growth on Si(1 0 0) but comparisons are made with growth on Si(1 1 1). The SiO_x/Si(1 1 1) interface is considered to have relatively more interface trapped charges and fixed oxide charges compared to the SiO_x/Si(1 0 0) interface (see for example the study by Vitkavage et al. [25]). The Si(1 1 1) orientation is therefore at present not the preferred substrate for MOSFETs. Depositing a metal oxide on top of the silicon substrate is however a different process compared to oxidizing the substrate atoms. STM studies have shown that the Si(1 1 1)-(7 × 7) reconstruction is locally more stable and easier to prepare with a small number of defects compared to the Si(1 0 0)-(2 × 1) reconstruction. Consequently, studies of the growth on the Si(1 1 1) surface make for most valuable comparisons. The results presented here reveal significant differences in the properties of the interfaces formed on the two surfaces, which is discussed in terms of surface termination and precursor fragmentation tendency.

2. Experimental

The measurements were performed at the bending magnet beamline D1011 at the Swedish synchrotron radiation source MAX II. The beamline consists of a Zeiss SX-700 monochromator and an end station dedicated to surface science experiments. The end station comprises a 200 mm radius hemispherical electron energy analyzer of Scienta type for photoemission measurements [26]. A multichannel plate was used to record XAS spectra by detection of secondary electrons. The end station also features a LEED for studies of surface ordering.

The n-doped (P) Si(1 0 0) wafers (Polishing Corp. of America, resistivity 0.1–1.0 Ω cm) were cleaned *ex situ* ultrasonically in acetone and ethanol. This step was followed by annealing in UHV to 1000 °C while keeping the pressure below 1×10^{-9} Torr. This resulted in a sharp (2 × 1) LEED pattern and a Si 2p PES spectrum characteristic for the Si(1 0 0)-(2 × 1) surface. Small amounts of carbon and oxygen were detected by surface sensitive core level photoemission.

The n-doped (P) Si(1 1 1) wafers (Virginia Semiconductors, resistivity 0.1–1.0 Ω cm) were first cleaned *ex situ* by employing a wet etching method [27] followed by repeated 5–10 s heating to 1150–1200 °C *in situ*. This resulted in a sharp (7 × 7) LEED pattern. No impurities were observable by PES.

Zirconium tetra *tert*-butoxide was used as single source precursor to deposit ZrO_2 films on Si(1 0 0)-(2 × 1) and Si(1 1 1)-(7 × 7) surfaces. In all cases the sample temperature was 400 °C during exposure to the precursor. The sample was exposed to ZTB via a dosing tube (10 mm in diameter) positioned a few mm from the sample surface. The high vacuum part of the ZTB dosing system was thoroughly baked out and passivated. Passivation of the high vacuum part was accomplished by exposing the system to ZTB without pumping. This was done in direct connection to the bake-out, while the system was still warm. The ZTB liquid was purified by multiple freeze–pump cycles. Prior to deposition on the Si samples, the UHV parts (chamber walls, dosing tube, etc.) were also subject to passivation. This was performed by admission of ZTB in the 10^{-7} mbar range for 10–20 min a couple of times. This procedure has been found to give very reproducible growth rates. The pressure during deposition was 2×10^{-8} mbar, read as the background pressure in the chamber. The local pressure at the sample surface is crudely estimated to be about 20 times higher.

The film thickness was estimated from the damping of the Si 2p PES signal measured at 758 eV photon energy. At this photon energy, the Si 2p photoelectron inelastic mean free path is about 20 Å. In ZrO_2 the electron inelastic mean free path at a kinetic energy of about 1387 eV, corresponding to that of Si 2p photoelectrons excited by Al Kα radiation, has previously been given as 25–30 Å [2,28]. Assuming a standard shape of the escape depth curve, a value close to 20 Å is obtained at 660 eV kinetic energy. We have confirmed that this value is reasonable by performing an independent film thickness measurement by X-ray reflection of an 80 Å thick film.

The spectra are normalized to the ring current and the number of scans unless stated otherwise. The binding

energy (BE) scale in the PES spectra are referenced to the Fermi level of the sample holder, unless stated otherwise. The photon energy (PE) scale in the XAS spectra is absolute, obtained by calibration to a PES feature excited by first and second order light.

3. Results

3.1. Growth rate

Fig. 1 shows the estimated film thickness as a function of ZTB exposure time. For film growth on Si(1 0 0)-(2 × 1) and Si(1 1 1)-(7 × 7) the film thickness for each situation is derived from the damping of the Si 2p PES bulk signal. Included in Fig. 1 is also a growth series on a Si-rich SiC(0 0 0 1)-(3 × 3) surface. The ZrO_2/SiC(0 0 0 1) system is discussed in detail elsewhere [29], and serves here as a valuable comparison when discussing the effect of having carbonaceous species present (see Section 3.2.3).

Common for film growth on the three different surfaces is that the growth rate is higher at the initial stages than at the later stages. The growth rates on the Si(1 0 0) and Si(1 1 1) surfaces are very similar up to a film thickness of about 30–40 Å after which the growth proceeds more rapidly on Si(1 1 1) than on Si(1 0 0).

A progressive decline in growth rate can be qualitatively understood by the formation of an extended interface layer followed by formation of stoichiometric ZrO_2. The ZTB molecule provides four oxygen atoms per zirconium atom. Thus, provided there are Si atoms that can be oxidized, each molecule can, in principle, yield one ZrO_2 unit and one SiO_2 unit. Si atoms that can be oxidized are present only during the initial stages of growth, resulting in the formation of an interface with graded composition. The interfacial Si concentration is expected to decrease with increasing film thickness due to the increased silicon and oxygen diffusion lengths required for silicon oxidation. Consequently, simply based on pure stoichiometric reasoning, a decrease in the growth rate by a factor of two is expected.

However, the reactivity of the surface towards ZTB decomposition may also vary depending on the surface composition, giving rise to a decreased growth rate. Furthermore, a changeover to a rougher morphology would also be observed as an apparent decrease in the growth rate when the film thickness is monitored in this way.

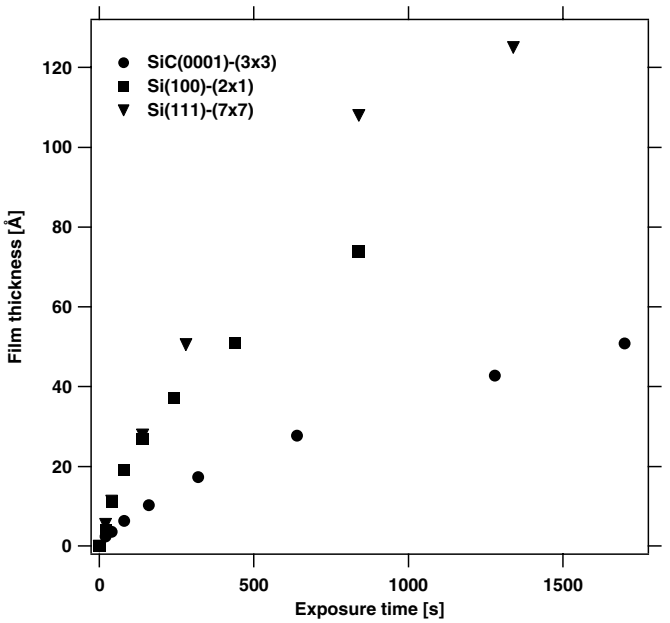

Fig. 1. Film thickness as function of ZTB exposure time derived from the attenuation of the Si 2p bulk signal. The pressure during dosing was 2×10^{-8} mbar, read as the background pressure. Results for growth on Si(1 0 0)-(2 × 1), Si(1 1 1)-(7 × 7) and SiC(0 0 0 1)-(3 × 3) are included.

3.2. Precursor related core level photoelectron spectra

3.2.1. Zr 3d

Zr 3d spectra obtained after film deposition on the Si(1 0 0) and Si(1 1 1) surfaces are shown in Fig. 2a and b. In all situations one spin-orbit pair having symmetric peaks is observed. For the thickest films on both surfaces the Zr $3d_{5/2}$ BE is 184.0 eV, which shifts towards lower values for thinner films. The shift amounts to about 0.6 eV and is related to the choice of BE reference. To clarify, the spectra are referenced to the Fermi level of the metallic sample holder. Using the vacuum level as BE reference gives another result, which we discuss in detail elsewhere (unpublished). The BE for the thick film is about 0.8 eV higher than previously reported for ZrO_2 films [11,15,19,20]. The BE difference is attributed to differences in the preparation conditions and the calibration procedure.[1] The results presented in Fig. 2 thus strongly suggest that only one Zr species exists throughout the deposition series and the BE value indicates that this species can be identified as Zr^{4+}.

3.2.2. O 1s

Fig. 3a and b show O 1s photoemission spectra for growth on Si(1 0 0) and Si(1 1 1), respectively. The two growth series are very similar: A single feature at binding energy 531.5 eV is strongly dominating for all situations. The binding energy is found to shift to higher values for increasing film thickness. The shift amounts to about 0.2–0.4 eV, with slightly higher values found upon growth on Si(1 1 1). A minor structure on the high binding energy side of the main peak at about 533.5 eV BE is observed in all O 1s spectra. The relative intensity of this feature is remarkably constant (6–9%) during the growth series on the two surfaces.

There are previous studies where it is argued that the O 1s BE of ZrO_2 is about 1.3–2 eV greater than the O 1s BE

[1] The referenced work often regard preparations that are not conducted under UHV conditions. The BE values are furthermore commonly referred to the Si 2p bulk BE measured for the clean sample, thereby excluding band bending effects. This procedure accounts for about 0.6 eV of the BE difference.

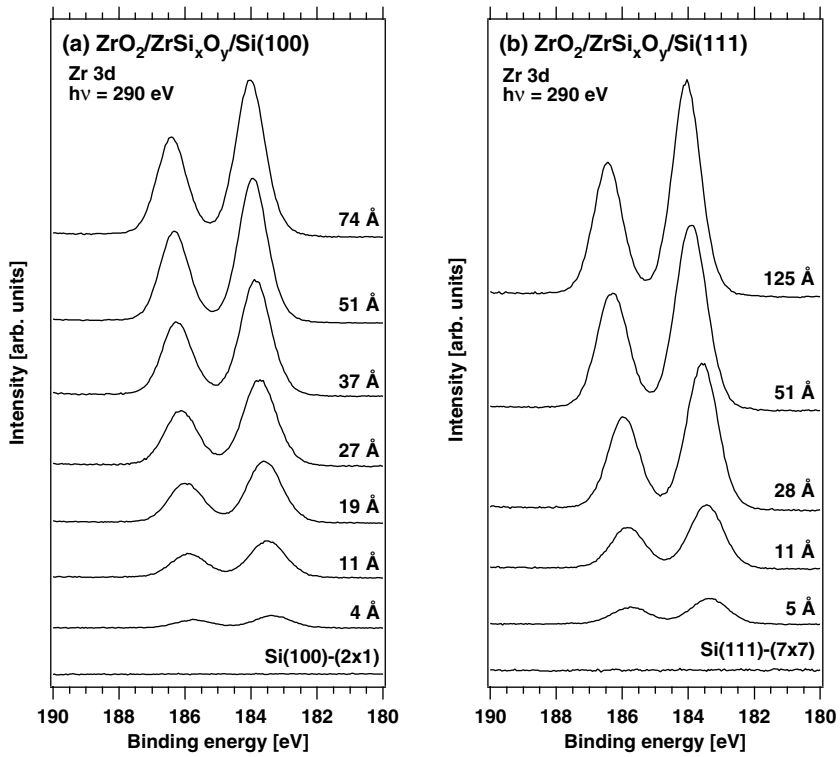

Fig. 2. Zr 3d photoelectron spectra from the deposition of $ZrO_2/ZrSi_xO_y$ on: (a) Si(100)-(2 × 1) and (b) Si(111)-(7 × 7).

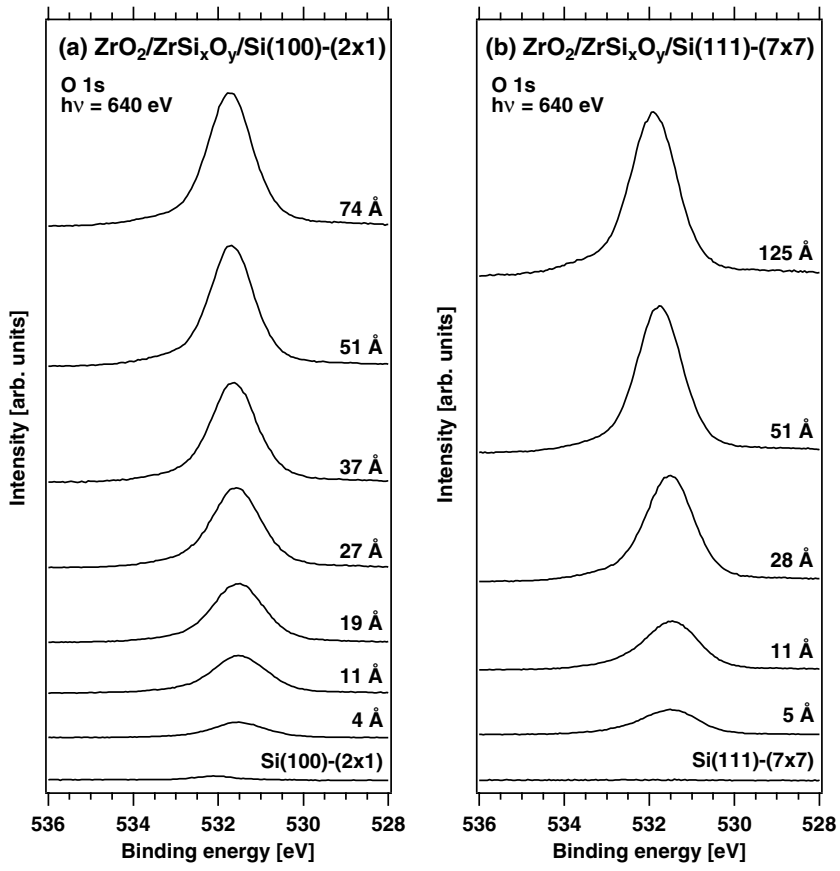

Fig. 3. O 1s photoelectron spectra from the deposition of $ZrO_2/ZrSi_xO_y$ on: (a) Si(100)-(2 × 1) and (b) Si(111)-(7 × 7).

of SiO_2 [2,15,20,30]. This would suggest two well-separated peaks if, e.g. a $ZrO_2/SiO_2/Si$ layered structure is formed. Formation of a silicate of the form $ZrSi_xO_y$ is on the other hand typically associated with only one O 1s peak of intermediate BE [30]. According to this view, the behavior in the present study is more in line with $ZrO_2/ZrSi_xO_y$ formation rather than the formation of a ZrO_2–SiO_2 system. However, we have also prepared thin SiO_x layers on Si(1 0 0) and Si(1 1 1) in order to compare the O 1s binding energy to that of the deposited ZrO_2 film. The BE differences are significantly smaller than those of the work cited above. The O 1s BE for SiO_x/Si(1 1 1) is 531.9 eV whereas the O 1s BE for ZrO_2/Si(1 1 1) is 531.5–532 eV depending on film thickness. The O 1s BE values for SiO_x/Si(1 0 0) and ZrO_2/Si(1 0 0) are 532.1 and 531.5–531.7 eV, respectively. The reason for the discrepancy is most probably related to different procedures for sample preparation and binding energy referencing. Based on the O 1s spectra alone it is therefore not possible to deduce whether the interface consists of a silicate ($ZrSi_xO_y$) with graded composition or a $ZrO_2/SiO_2/Si$ layered structure.

The identity of the weak feature of 533.5 eV BE is more nebulous. A probable assignment is that it stems from hydroxyl groups formed upon precursor decomposition. The presence of hydroxyl groups has been discussed in previous studies and it has been proposed that their presence significantly enhances the surface reactivity towards precursor decomposition and hence increases the growth rate [12].

Another possible assignment is a state associated with oxygen atoms not being in the proper bulk configuration, i.e. defect states. Sakamoto et al. [31] have studied the initial dry oxidation process of the Si(1 1 1)-(7 × 7) surface using high-resolution O 1s core-level measurements and an extra O 1s component of about 532.5 eV BE was observed even after annealing to 600 K.

3.2.3. C 1s

Fig. 4a and b show the C 1s spectra recorded upon growth on the two surfaces. Table 1 summarizes the labeling and assignment of the C 1s components as discussed below. We will first consider growth on the Si(1 0 0) surface. The spectrum for the pristine Si(1 0 0)-(2 × 1) surface exhibits a weak, broad feature (FWHM about 2 eV) centered at a BE of 283.6 eV. This is due to small amounts of surface contamination. For simplicity, this weak structure will not be considered in the following discussion. Upon film deposition, the C 1s spectrum for every situation up to 74 Å is well described by three different carbon species denoted C1–C3 in Fig. 4a. The binding energies for the first few depositions are 283.6 eV (C1), 284.4 eV (C2) and

Table 1
Labeling and assignment of C 1s photoelectron spectra for growth of $ZrO_2/ZrSi_xO_y$ on Si(1 0 0)-(2 × 1) and Si(1 1 1)-(7 × 7)

Surface	Label	C 1s	Binding energy (eV)
Si(1 0 0)	C1	Si–C	283.6
	C2	Si–C–C–Si	284.4
	C3	$–CH_3$	285.3
Si(1 1 1)	C12	Si_xC_y	284.0–284.4
	C3	$–CH_3$	285.3
	C4	C–O	287.4

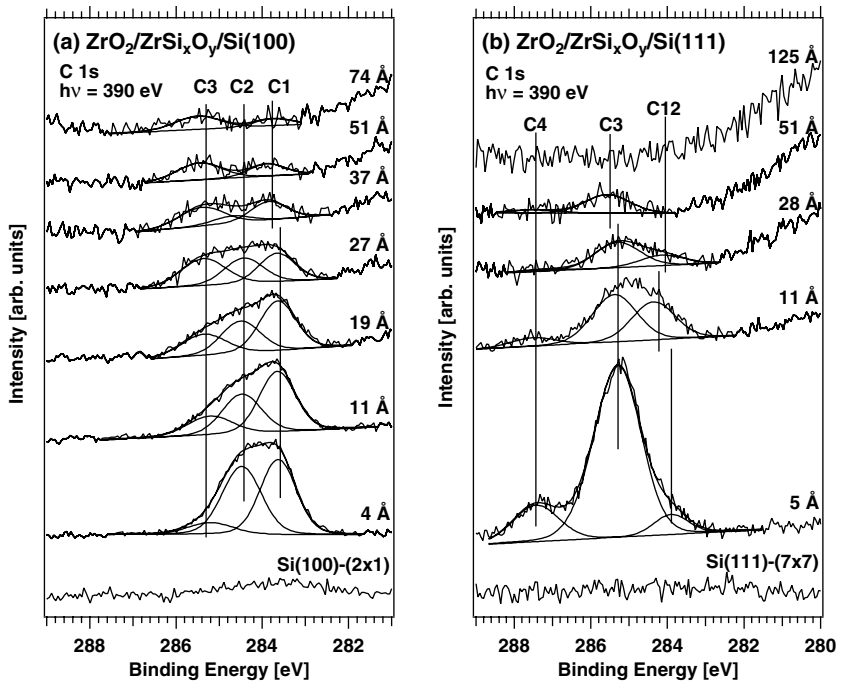

Fig. 4. C 1s photoelectron spectra from the deposition of $ZrO_2/ZrSi_xO_y$ on: (a) Si(1 0 0)-(2 × 1) and (b) Si(1 1 1)-(7 × 7). The different surface species are labeled.

285.3 eV (C3), respectively. However, shifts of about +0.2 eV are observed when increasing the film thickness.

Different carbon species can be discerned also during growth on Si(1 1 1)-(7 × 7). The most apparent difference as compared to growth on Si(1 0 0) is the peak at highest binding energy (287.4 eV). This state, denoted C4, is not found in the data set for Si(1 0 0). The next peak has a binding energy of 285.4 eV. It is denoted C3, since the binding energy is similar to that of species C3 observed upon growth on Si(1 0 0). There are also states that fall within the binding energy range (283.6–284.4 eV) defined by peaks C1 and C2 observed upon growth on Si(1 0 0). However, in the case of growth on Si(1 1 1) it is not possible to discern two well-defined states, possibly due to the higher relative intensity of peak C3. The feature is therefore denoted C12 in order to indicate the connection to peaks C1 and C2.

The C 1s peaks found at highest binding energy (C4 and C3) can be assigned to the two different kinds of carbon found within a *t*-butoxy species. Peak C4 is due to emission from the inner C atom bonded to O while peak C3 is due to emission from methyl groups. The BE values are in good agreement with those reported for the same C species within 2,3-butanediol on Si(1 0 0), when taking the different BE calibration into account[1] [32]. In passing, we note that peak C3 has an asymmetric line profile. The asymmetry could originate in the vibrational progression typical for methyl groups, which has previously been resolved in C 1s spectra for adsorbed ethylidyne [33,34].

The formation of C–Si bonds gives rise to C 1s features at 284.6–283.9 eV [35,36]. Therefore the peaks C1 and C2 are most probably the result of *t*-butoxy fragmentation. The detailed assignment of peaks C1 and C2 is however more uncertain. Adsorption of ethylene in an sp^3-configuration on both Si(1 0 0)-(2 × 1) and Si(1 1 1)-(7 × 7) results in a C 1s peak at about 284 eV binding energy [37]. Decomposition of this species by heating results in a C 1s state of about 283 eV BE [37]. Based on this, we propose that peak C2 can be attributed to –C–C– species bonded to Si, whereas peak C1 is due to carbidic carbon atoms.

The integrated intensities of the C 1s peaks as a function of film thickness on Si(1 0 0)-(2 × 1) and Si(1 1 1)-(7 × 7) are plotted in Fig. 5a and b, respectively. The intensity values are in relative terms and the values in Fig. 5a can be compared to those in Fig. 5b. Determining the carbon coverage in absolute terms is however much more difficult. To at least give a rough estimate, a value of 1.8 on the scale in Fig. 5 corresponds to a carbon amount that is about 15–25% of the amount of oxygen in a SiO_x layer formed on Si(1 0 0).[2]

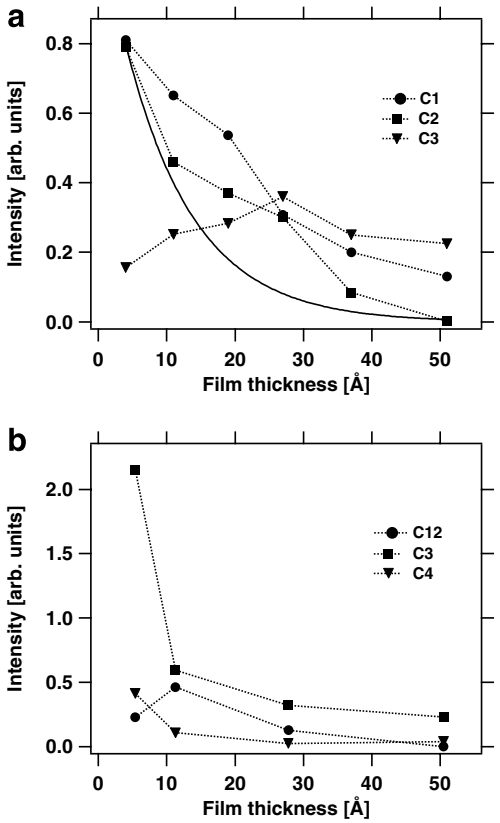

Fig. 5. Integrated intensities of the different C 1s components as a function of $ZrO_2/ZrSi_xO_y$ film thickness on: (a) Si(1 0 0)-(2 × 1) and (b) Si(1 1 1)-(7 × 7). The solid line represent the attenuation expected upon additional film deposition. The mean free path was set to 10 Å.

Starting with the growth on Si(1 0 0)-(2 × 1), it is observed that the intensity of peaks C1 and C2 decreases monotonically with film thickness. The behavior of peak C3 is significantly different: The intensity increases slightly up to a film thickness of 30 Å after which the intensity starts to drop. For comparison, Fig. 5a also shows the expected attenuation of the signal imposed by the additional film deposited in the subsequent steps. The mean free path is set to 10 Å and the initial intensity is set to 0.8, corresponding to the intensity of peaks C1 and C2 after the first deposition. The intensity decrease of peaks C2 and C1 are slower than expected from the attenuation curve. This implies either that the C1 and C2 species continues to form (but to a smaller extent) or that film growth is locally slower on the carbon contaminated patches. That the presence of carbon may reduce the growth rate is indicated by the considerably lower growth rate found on the SiC substrate, as shown in Fig. 1.

Thus, we propose that species C1 and C2, which are associated with carbonaceous ligand fragments of the ZTB molecule, are primarily formed during the first deposition step. This is not unexpected, given the high reactivity of the Si(1 0 0)-(2 × 1) surface.

Continuing with the growth on Si(1 1 1)-(7 × 7), it is found that species C3 is more abundant after the first

[2] The carbon coverage was estimated for the deposition of 5 Å $ZrO_2/ZrSi_xO_y$ on Si(1 0 0). The C 1s total integrated intensity (approx. 1.8 on the scale in Fig. 4a) was related to the O 1s integrated intensity, giving a stoichiometric ratio O/C = 6. The O 1s intensity was in turn related to the O 1s intensity after formation of 6 Å SiO_x on Si(1 0 0) by exposure to O_2 at 420 °C.

deposition steps as compared to growth on Si(100). However, the intensity of peak C3 decreases dramatically between 4 and 11 Å. It is also noted that the relative decrease in the intensity of peak C4 is equal to that of peak C3. The relative intensity decrease of peaks C3 and C4 between the first and the second deposition step is 73%, which is much larger than if only damping due to deposition of additional material is taken into account (at most 50%). In contrast, peak C12 increases slightly between 4 and 11 Å. For the following deposition steps all three peaks decrease progressively. This suggests that no additional carbonaceous ligand fragments are formed after a film thickness of 11 Å.

3.3. Substrate core level photoelectron spectra

Fig. 6 shows Si 2p spectra for three different situations: 4 Å SiO_x/Si(100), 51 Å ZrO_2/$ZrSi_xO_y$/Si(100) and 51 Å ZrO_2/$ZrSi_xO_y$/Si(111). The spectra were recorded at a photon energy of 130 eV, giving a very high surface sensitivity. The Si 2p bulk peak undergoes BE shifts upon film deposition. The reason for the shift upon ZrO_2 growth on Si(100) has been discussed in detail elsewhere [24]. Briefly, the BE shift vs. the Fermi level stems from the annihilation of the band gap states associated with the (2×1) surface reconstruction. In Fig. 6, the binding energy scale is relative to the bulk peak to facilitate the comparison between the different situations. Table 2 summarizes typical results from curve fits of the spectra obtained after ZTB exposure.

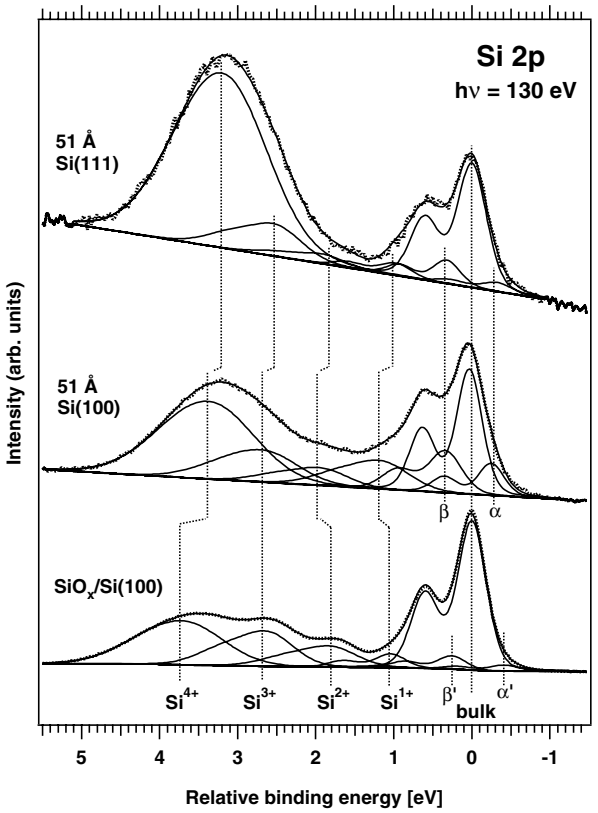

Fig. 6. Si 2p photoelectron spectra from the deposition of 51 Å ZrO_2/$ZrSi_xO_y$ on Si(100)-(2×1) and 51 Å ZrO_2/$ZrSi_xO_y$ Si(111)-(7×7). For comparison, the spectrum obtained after oxidation of the Si(100)-(2×1) by O_2 is shown at the bottom. The different forms of Si are labeled.

We will first consider the SiO_x/Si interfaces. The Si 2p spectra for the SiO_x/Si(100) and the SiO_x/Si(111) interfaces both contains five distinguishable spin-orbit pairs attributed to bulk, Si^{1+}, Si^{2+}, Si^{3+} and Si^{4+} species [38]. For the SiO_x/Si(100) interface there are two additional weak states labeled α' and β' in Fig. 6. The α' and β' states are positioned on each side of the bulk peak and the relative intensities compared to the bulk peak are 0.04 (α') and 0.08 (β'). The origin of these features has previously been discussed in terms of silicon atoms in strained bulk coordination [39]. It is likely that similar states also are formed upon oxidation of Si(111), but no detailed investigation has been performed so far.

The Si 2p spectra for ZrO_2/$ZrSi_xO_y$/Si(100) require the inclusion of states similar but not identical to the α' and β' states of the SiO_x/Si(100) interface. Fits of high accuracy were possible to obtain when assuming that these states have a constant lineshape and a constant energy separation with respect to the bulk peak. The separations vs. the bulk peak as well as the linewidths were however found to be different from the α' and β' peaks. To stress this difference, the features are denoted α and β. The difference most likely stems from the fact that the surface is now exposed to a metal organic molecule and not to pure oxygen. A Si 2p component at the same position as β has for example been found upon adsorption of hydrocarbons [37,40,41], possibly including Si-H formations. Silicon atoms bonded to carbon in a SiC-like local geometry can furthermore give rise to a Si 2p signal in the same binding energy region as α [37], and it is reasonable that second nearest neighbor silicon atoms to such a site have a binding energy not exactly equal to the bulk peak.

The intensity ratio between the α component and the bulk component increases up to an overlayer thickness of 19 Å, and is from this point on fairly constant ($I_\alpha/I_{bulk} = 0.25 \pm 0.05$). The intensity ratio between the β component and the bulk component is fairly constant

Table 2
Typical results obtained by curve fitting of the Si 2p spectra for ZrO_2/$ZrSi_xO_y$ on Si(100) and Si(111)

Component	Shift (eV)	Gaussian width (FWHM) (eV)
α	−0.25	0.35
β	+0.29	0.47
Bulk	0.00	0.35
Si^{1+}	+1.15	0.75
Si^{2+}	+1.90	0.75
Si^{3+}	+2.55	1.01
Si^{4+}	+3.20	1.15

The Si 2p spectra have been fitted using a maximum of seven spin-orbit pairs for which the branching ratio is set to 0.5, the Lorentzian life-time broadening is set to 0.085 eV and the spin-orbit split is set to 0.602 eV [23]. The shifts are given relative to the bulk component.

($I_\beta/I_{bulk} = 0.42 \pm 0.05$) for overlayer thicknesses ranging from 4 to 51 Å. The Si 2p spectra corresponding to 74 Å overlayer thickness is relatively noisy but it is clear that the β component is still present.

The α and β components reach a higher relative intensity vs. the bulk peak than found for the α' and β' components for SiO_x/Si(100). This is consistent with the dramatically increased amount of oxidized Si and the additional formation of hydrocarbon fragments. The relative intensity of the β component is comparable to that of the dimers for the clean Si(100)-(2 × 1) surface (as fitted by the model suggested by Landemark et al. [42]). That is, the amount of the β species is of the order of one monolayer. Analogously, the α species amounts to slightly less than one monolayer. However, a larger data set including angular scans is needed to determine the depth distribution of these species more accurately. It is furthermore interesting to note that the bulk, α and β components exhibit essentially the same attenuation behavior upon film growth. This indicates that the species responsible for the α and β component are primarily formed at the initial stages of the film growth and are thereafter retained as more material is added.

Finally, the proximity of the α and β peaks to the bulk peak makes an accurate curve fitting difficult. To improve the accuracy, a Si 2p spectrum was recorded using 390 eV photons for each situation. This gives a comparably less surface sensitive measurement. Compared to the measurement performed using 130 eV photons the relative intensities of the α and β components are reduced by more than 50% and thereby the linewidth of the bulk component is more clearly revealed. This further motivates the need to include the α and β components.

Turning next to the oxidized forms of Si, it is found that the Si^{1+} component is broader in comparison to that of the SiO_x/Si(100) interface. We find it reasonable that the Si^{1+} component for the situations after ZTB exposure is actually composed of more than one component, e.g. one attributed to Si^{1+} in SiO_x/Si(100) cross-linking and another attributed to interaction with hydrocarbons and/or ZrO_x. The intensity ratio between the Si^{1+} and bulk components is furthermore larger in the Si 2p spectra corresponding to situations after ZTB exposure compared to the spectra for the SiO_x/Si(100) interface.

The Si^{3+} component progressively increases relative to the bulk component with exposure for the growth on Si(100). At the overlayer thickness of 51 Å the intensity ratio between the Si^{3+} and the bulk components is higher than the intensity ratio measured for the SiO_x/Si(100) interface, and at the overlayer thickness of 74 Å the intensity ratio has increased even further. This indicates that the Si^{3+} species is not only associated with $ZrSi_xO_y$–Si(100) linkage, it is also distributed within the extended $ZrSi_xO_y$ interfacial layer.

The Si^{4+} component is shifted towards the bulk peak for situations after ZTB exposure compared to the corresponding position found for the SiO_x/Si(100) interface. This behavior has previously been attributed to silicate formation [43,44] of the form $ZrSi_xO_y$.

The behavior of the oxidized silicon species upon film growth is best described by the graded composition $ZrSi_xO_y$ interface model. The expected spectral signature of a ZrO_2/SiO_2/Si(100) layered structure with sharp interfaces is not obtained. It should however be noted that the interface structure most likely depends on the sample preparation conditions.

The Si 2p spectra recorded upon film growth on Si(111) have been decomposed in a similar manner. Also in the case of $ZrO_2/ZrSi_xO_y$/Si(111) the inclusion of the α and β components is necessary. For 51 Å film thickness, the relative α and β intensities vs. the bulk peak are however lower than for 51 Å deposited on Si(100). At a total film thickness of 51 Å, a larger part of the overlayer is attributed to Si^{4+} species for growth on the Si(111) substrate compared to the growth on the Si(100) substrate, see Fig. 6. On the other hand, the relative intensities of the beta, Si^{1+} and Si^{2+} species are smaller for growth on Si(111) compared to growth on Si(100).

3.4. X-ray absorption spectra

In the case of a 74 Å thick film grown on Si(100), independent XRD measurements (not shown) give evidence for formation of tetragonal ZrO_2. Formation of the tetragonal polymorph at 400 °C agrees with previous studies [10]. An inherent feature of core level XAS spectra is that they are sensitive to changes in the local geometric structure, i.e. at the atomic site of the core excitation. From this follows that the Zr 3p and O 1s XAS spectra for this situation can be considered as fingerprints for the *t*-ZrO_2 local structure. Zr 3p XAS spectra for increasing film thickness on Si(100) (a) and Si(111) (b) are depicted in Fig. 7. The corresponding O 1s XAS spectra are shown in Fig. 8. Upon comparison, we can conclude that also the spectra measured for thickest film deposited on Si(111) carry the signature of *t*-ZrO_2.

For thinner films, there is a clear difference in the behavior on the two surfaces. This is most clearly seen at the O 1s edge in the photon energy range 542–550 eV. The states characteristic of *t*-ZrO_2 within this energy range are indicated with vertical lines in Fig. 8. The O 1s XAS spectrum recorded upon deposition on Si(100) contains the structures of *t*-ZrO_2 already at a film thickness of 11 Å, albeit broadened. Upon deposition on Si(111) these features are not observed at a thickness of 28 Å. In this series, the signature of *t*-ZrO_2 is first observed at a film thickness of 51 Å. Consequently, upon film deposition using ZTB at 400 °C the local structure typical for *t*-ZrO_2 forms at an earlier stage on Si(100) than on Si(111).

The Zr–O interaction in the $ZrSi_xO_y$ interface could be very different from that in bulk ZrO_2. This could be the result of a different Zr–O coordination. However, a difference in overlap could also occur due to electronic and geometric effects without changing the coordination number. Relative

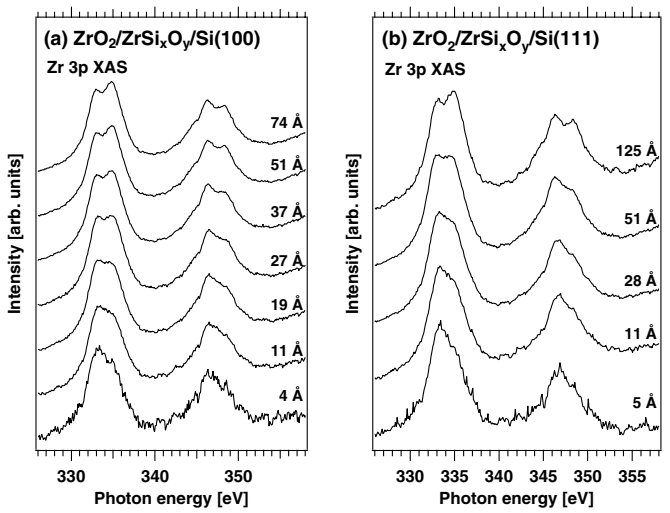

Fig. 7. Zr 3p X-ray absorption spectra from the deposition of ZrO_2/$ZrSi_xO_y$ on: (a) Si(100)-(2 × 1) and (b) Si(111)-(7 × 7).

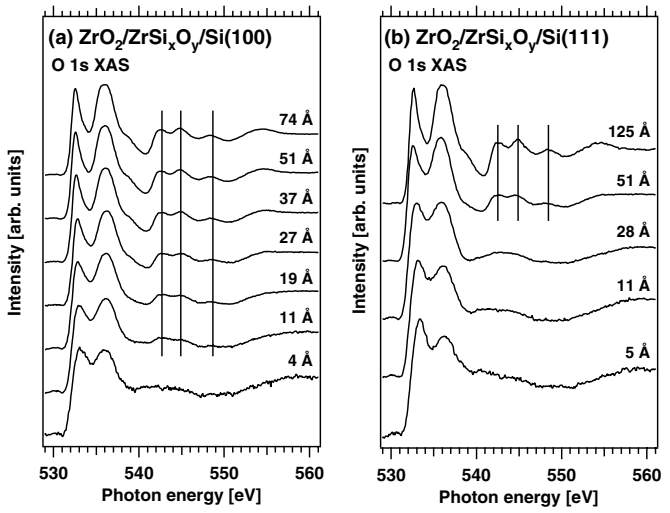

Fig. 8. O 1s X-ray absorption spectra from the deposition of ZrO_2/$ZrSi_xO_y$ on: (a) Si(100)-(2 × 1) and (b) Si(111)-(7 × 7).

changes in the Zr–O interaction can be traced by the ratio between the Zr $3p_{3/2}$ XAS peak and the purely Zr 4d–O 2p related O 1s XAS feature at about 532.6 eV [24]. The O/Zr intensity ratios obtained this way are shown in Fig. 9. We stress that the values are relative values and do not correspond to absolute stoichiometric values. In the case of growth on Si(100), it is observed that the O/Zr XAS ratio is constant up to a film thickness of 20 Å after which it increases progressively. This is consistent with a Zr–O overlap that is lower in the interface than in stoichiometric ZrO_2 since the increase starts at the point of interface completion [24]. The relative increase in the O/Zr ratio between 19 and 74 Å is about 30%. In the case of growth on Si(111), the O/Zr ratio is at the first stages very similar to the values for growth on Si(100). The increase does however not set in until a film thickness of about 50 Å is reached. The relative increase from 50 to 125 Å is 31%,

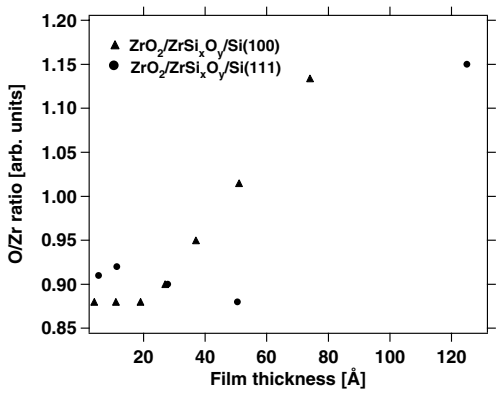

Fig. 9. Intensity ratios obtained by dividing the leading features in the Zr 3p and O 1s X-ray absorption spectra. The plots represent relative changes on the Zr–O hybridization and do not correspond to absolute stoichiometric values.

which is basically the same as that observed for Si(100) between 19 and 74 Å.

4. Discussion

4.1. Surface chemistry of carbonaceous species

The results show no sign of a C 1s peak associated with C–O bonds upon growth on the Si(100) surface. This excludes the presence of *t*-butoxy surface species at a temperature of 673 K. Previous studies are in agreement with this conclusion. In a TPD study of *t*-butanol on Si(100) desorption of isobutene was observed at 640 K, which was taken as evidence for C–O scission [45]. Likewise, the stability of *t*-butoxy on ZrO_2 during steady state growth is low [12]. Growth above 573 K is assumed to proceed by hydrogen elimination and formation of isobutene that desorbs, leaving hydroxyl groups on the surface [12]. The presence of an O 1s feature of 533.5 eV BE lends support to a mechanism in which formation surface hydroxyl groups occurs.

Methyl groups are found on the surface and a very weak C 1s feature due to methyl groups is detected even after deposition of a 74 Å thick film. The point at which the methyl C 1s peak reaches its maximum coincides with the previously estimated point of interface completion. That is, the probability for having surface species containing methyl groups decreases once the intermixing has ended, which in turn suggests that this species requires the presence of Si surface atoms. This can be explained in terms of stable CH_3-groups on SiO_x or on defects on the mixed surface. The defects are expected to decrease once an extended ZrO_2 film forms. However, it should be noted that the C 1s peak due to methyl groups never reaches zero intensity in the film thickness range studied here but it is possible that the surface methyl groups completely disappear at even thicker films, as observed for Si(111).

Finally, the C 1s spectra show that carbonaceous fragments are formed on the Si(100) surface during the first

stages of film growth. Due to the reactivity of the Si(100) surface, the ligand reaction products cannot desorb effectively as isobutene. The carbon fragments thus become incorporated within the first few Å of the interface. The attenuation behavior of the α and β components in the Si 2p spectra are furthermore correlated to that of the C 1s peaks associated with carbonaceous fragments. This suggests that the enhanced intensity of the α and β features can be attributed to non-oxidized silicon atoms interacting with hydrocarbons.

On the Si(111) surface the processes are very different. A C 1s peak due to C–O bonds is observed up to a film thickness of about 11 Å. A strong peak due to methyl groups is furthermore observed. This suggest that intact *t*-butoxy groups remain on the Si(111) surface, which is not the case upon growth on Si(100). This is also observed as a lower intensity of the C 1s peak due to carbonaceous fragments as compared to the Si(100) surface. The C 1s peaks associated with C–O and $-CH_3$ carbon decrease however dramatically between 4 and 11 Å. The decrease is larger than expected from the coverage of subsequent film. This suggests that the *t*-butoxy groups are not stable and react upon further exposure to ZTB in order to form species that desorb.

4.2. Oxide formation

The data demonstrate significant differences in the interfacial local geometric structure depending on the Si crystal face. The Si 2p spectra show that the relative amount of Si in intermediate oxidation states (+1, +2 and +3) is larger on Si(100) than on Si(111). This result shows that there are differences in the ZrO_2–SiO_x linkage.

In the case of deposition on Si(100) the XAS data suggest that the ZrO_2 local structure does not change to a large extent from a film thickness of 11 Å and upwards. However, there are several indications that a film thickness of about 30 Å defines a critical point [24], but at this film thickness no dramatic change in the XAS spectral shape can be discerned. In contrast, the O/Zr XAS intensity ratio displays a steep increase with an onset at about 30 Å. The interpretation is that electronic effects due to the presence of SiO_x or ZrO_2 neighboring units play an important part. The Zr–O interaction is expected to be very different in a film with mixed composition as compared to a homogeneous film. This can in a simple picture be discussed in terms of the different electronegativities of Si and Zr. Calculations of the *t*-ZrO_2 and $ZrSiO_4$ electronic structures show that the Zr–O hybridization is weaker in $ZrSiO_4$ than in *t*-ZrO_2 [46]. Intermixing with SiO_x thus induces a localization of the Zr 4d states reducing the hybridization with the O 2p states. The increase in the O/Zr ratio as witnessed by XAS is therefore an electronic effect induced by changes in the composition of the film rather than changes in the local Zr–O geometric structure.

This is in contrast to the behavior upon deposition on Si(111). In this case, the *t*-ZrO_2 signature is not observed until after a deposition of 51 Å and the increase in the O/Zr intensity ratio occurs after this point. Thus, the local structure associated with *t*-ZrO_2 is not formed in the film thickness range were intermixing occurs.

A recent study employing model calculations points out a fundamental difference in the prerequisites for ZrO_2 growth on Si(100) and Si(111), namely the matching of the number of dangling bonds (DB) to the Zr and O valency [47]. On Si(100), each surface Si atom has two DBs. When brought into contact with an O-terminated ZrO_2-layer, the O atoms form two Si-O bonds to the DBs. In this way, the interface valence condition can be satisfied and the surface is compatible with ZrO_2 epitaxy. The valence condition can in principle also be satisfied for a Zr-terminated layer, where the Zr forms two polar bonds with the two Si DBs. The latter geometry is however incompatible with our results as the Zr 3d spectra show no evidence for reduced Zr species due to Zr–Si bond formation.

On Si(111) each surface Si atom only provides a single DB. Consequently, an extra 0.5 ML of oxygen must be added upon interface formation in order to satisfy the valence conditions. From this point of view, epitaxial growth of ZrO_2 is therefore a more complicated process. With respect to the present results, the theoretical study thus provides a plausible explanation as to why epitaxial ZrO_2 units can form already at a very early stage of film growth on Si(100), while a more amorphous ZrO_2 geometry dominates the early stages of growth on Si(111). However, the theoretical study does only consider a pure Si–ZrO_2 interface. The ligand fragments present in the case of ZTB-mediated growth may in the present case be important with regard to the geometrical properties at the initial stages of growth.

5. Summary

The growth of ultrathin ZrO_2 films on Si(100)-(2 × 1) and Si(111)-(7 × 7) has been studied with core level photoelectron spectroscopy and X-ray absorption spectroscopy. The films have been deposited at 400 °C sample temperature by chemical vapor deposition using zirconium tetra-*tert*-butoxide as precursor.

On Si(100)-(2 × 1) the local geometric structure characteristic for tetragonal ZrO_2 (*t*-ZrO_2) is clearly observed already at a film thickness of 11 Å and this structure remains up to the thickest film in this study (74 Å). It is observed that the Zr–O hybridization within the ZrO_2 unit depends on the chemical composition of the surrounding. This is most likely an effect of the different electronegativities of Zr and Si. On Si(111)-(7 × 7) the local structure of *t*-ZrO_2 is not observed until a film thickness of 51 Å is reached. The higher tendency for the formation of *t*-ZrO_2 on Si(100) can be related to the fact that the number of dangling bonds per surface Si atom agrees with the Zr–O valency, whereas the number of dangling bonds per surface atom on Si(111) does not.

The *t*-butoxy ligands undergo efficient C–O scission on Si(1 0 0), leaving carbonaceous fragments embedded in the interfacial layer. In contrast, after small deposits on Si(1 1 1) stable *t*-butoxy groups are found. These are consumed upon further deposition. Stable methyl and, possibly, also hydroxyl groups are found on both surfaces within a wide film thickness range.

Acknowledgements

The authors acknowledge the assistance from the MAX-lab staff and the financial support from the Swedish Science Council (VR) and the Göran Gustafsson Foundation.

References

[1] G.D. Wilk, R.M. Wallace, J.M. Anthony, J. Appl. Phys. 89 (2001) 5243.
[2] J.P. Chang, Y.-S. Lin, S. Berger, A. Kepten, R. Bloom, S. Levy, J. Vac. Sci. Technol. B 19 (2001) 2137.
[3] B.-O. Cho, J.P. Chang, Appl. Phys. Lett. 93 (2003) 745.
[4] M. Ritala, M. Leskelä, L. Niinistö, P. Haussalo, Chem. Mater. 5 (1993) 1174.
[5] M. Ritala, K. Kukli, A. Rahtu, P.I. Räisänen, M. Leskelä, T. Sajavaara, J. Keinonen, Science 288 (2000) 319.
[6] R.C. Smith, T. Ma, N. Hoilien, L.Y. Tsung, M.J. Bevan, L. Colombo, J.T. Roberts, S.A. Campbell, W.L. Gladfelter, Adv. Mater. Opt. Electron. 10 (2000) 105.
[7] J.-H. Choi, H.-G. Kim, S.-G. Yoon, J. Mater. Sci.: Mater. Electron. 3 (1992) 87.
[8] H. Yamane, T. Hirai, J. Mater. Sci. Lett. 6 (1987) 1229.
[9] R.C. Smith, N. Hoilien, C.J. Taylor, T. Ma, S.A. Campbell, J. Roberts, M. Copel, D.A. Buchanan, M. Gribelyuk, W.L. Gladfelter, J. Electrochem. Soc. 147 (2000) 3472.
[10] D.J. Burleson, J.T. Roberts, W.L. Gladfelter, S.A. Campbell, R.C. Smith, Chem. Mater. 14 (2002) 1269.
[11] J.P. Chang, Y.-S. Lin, K. Chu, J. Vac. Sci. Technol. B 19 (2001) 1782.
[12] M.A. Cameron, S.M. George, Thin Solid Films 348 (1999) 90.
[13] Z. Song, L.M. Sullivan, B.R. Rogers, J. Vac. Sci. Technol. A 23 (2005) 165.
[14] Y.-S. Lin, R. Puthenkovilakam, J.P. Chang, C. Bouldin, I. Levin, N.V. Nguyen, J. Ehrstein, Y. Sun, P. Pianetta, T. Conard, W. Vandervorst, V. Venturo, S. Selbrede, J. Appl. Phys. 93 (2003) 5945.
[15] T.S. Jeon, J.M. White, D.L. Kwong, Appl. Phys. Lett. 78 (2001) 368.
[16] R. Puthenkovilakam, J.P. Chang, Appl. Phys. Lett. 84 (2004) 1353.
[17] C. Krug, G. Lucovsky, J. Vac. Sci. Technol. A 22 (2004) 1301.
[18] Z. Song, B.R. Rogers, N.D. Theodore, J. Vac. Sci. Technol. A 22 (2004) 711.
[19] S.-S. Huang, T.-B. Wu, J. Vac. Sci. Technol. B 22 (2004) 1940.
[20] S. Miyazaki, M. Narasaki, M. Ogasawara, M. Hirose, Solid State Electron. 46 (2002) 1679.
[21] A. Sandell, M.P. Andersson, Y. Alfredsson, M.K.-J. Johansson, J. Schnadt, H. Rensmo, H. Siegbahn, P. Uvdal, J. Appl. Phys. 92 (2002) 3381.
[22] A. Sandell, M.P. Andersson, M.K.-J. Johansson, P.G. Karlsson, Y. Alfredsson, J. Schnadt, H. Siegbahn, P. Uvdal, Surf. Sci. 530 (2003) 63.
[23] P.G. Karlsson, J.H. Richter, M.P. Andersson, J. Blomquist, H. Siegbahn, P. Uvdal, A. Sandell, Surf. Sci. 580 (2005) 207.
[24] A. Sandell, P.G. Karlsson, J.H. Richter, J. Blomquist, P. Uvdal, T.M. Grehk, Appl. Phys. Lett. 88 (2006) 132905.
[25] S.C. Vitkavage, E.A. Irene, H.Z. Massoud, J. Appl. Phys. 68 (1990) 5262.
[26] J.N. Andersen, O. Björneholm, A. Sandell, R. Nyholm, J. Forsell, L. Thånell, A. Nilsson, N. Mårtensson, Synchrotron Radiat. News 4 (1991) 15.
[27] A. Ishizaka, Y. Shiraki, J. Electrochem. Soc. 133 (1986) 666.
[28] C.J. Powell, A. Jablonski, AIP Conf. Proc. 683 (2003) 321.
[29] P.G. Karlsson, L.I. Johansson, J.H. Richter, C. Virojanadara, J. Blomquist, P. Uvdal, A. Sandell, J. Appl. Phys., to be published.
[30] M.J. Guittet, J.P. Crocombette, M. Gautier-Soyer, Phys. Rev. B 63 (2001) 125117.
[31] K. Sakamoto, H.M. Zhang, R.I.G. Uhrberg, Phys. Rev. B 68 (2003) 075302.
[32] J.W. Kim, M. Carbone, M. Tallarida, J.H. Dil, K. Horn, M.P. Casaletto, R. Flammini, M.N. Piancastelli, Surf. Sci. 559 (2004) 179.
[33] J.N. Andersen, A. Beutler, S.L. Sorensen, R. Nyholm, B. Setlik, D. Heskett, Chem. Phys. Lett. 269 (1997) 371.
[34] A. Sandell, A. Beutler, A. Jaworowski, M. Wiklund, K. Heister, R. Nyholm, J.N. Andersen, Surf. Sci. 415 (1998) 411.
[35] A. Fink, W. Widdra, W. Wurth, C. Keller, M. Stichler, A. Achleitner, G. Comelli, S. Lizzit, A. Baraldi, D. Menzel, Phys. Rev. B 64 (2001) 045308.
[36] H. Liu, R. Hamers, Surf. Sci. 416 (1998) 354.
[37] F. Rochet, F. Jolly, F. Bournel, G. Dufour, F. Sirotti, J.-L. Cantin, Phys. Rev. B 58 (1998) 11029.
[38] F.J. Himpsel, F.R. McFeely, A. Taleb-Ibrahimi, J.A. Yarmoff, G. Holllinger, Phys. Rev. B 38 (1988) 6084.
[39] S. Dreiner, M. Schürmann, C. Westphal, Phys. Rev. Lett. 93 (2004) 126101.
[40] M.N. Piancastelli, J.J. Paggel, Chr. Weindel, M. Hasselblatt, K. Horn, Phys. Rev. B 56 (1997) R12737.
[41] M. Carbone, M.N. Piancastelli, J.J. Paggel, Chr. Weindel, K. Horn, Surf. Sci. 412/413 (1998) 441.
[42] E. Landemark, C.J. Karlsson, Y.-C. Chao, R. Uhrberg, Phys. Rev. Lett. 69 (1992) 1588.
[43] G.D. Wilk, R.M. Wallace, J.M. Anthony, J. Appl. Phys. 87 (2000) 484.
[44] J.P. Chang, Y.-S. Lin, Appl. Phys. Lett. 79 (2001) 3824.
[45] J. Kim, K. Kim, K. Yong, J. Vac. Sci. Technol. A 20 (2002) 1582.
[46] R. Puthenkovilakam, E.A. Carter, J.P. Chang, Phys. Rev. B 69 (2004) 155329.
[47] P.W. Peacock, J. Robertson, Phys. Rev. Lett. 92 (2004) 057601.